Super-collimation and negative refraction in hyperbolic Van der Waals superlattices

Sreekanth, Kandammathe Valiyaveedu; Simpson, Robert E.

2019

Sreekanth, K. V., & Simpson, R. E. (2019). Super-collimation and negative refraction in hyperbolic van Der waals superlattices. Optics Communications, 440, 150-154. doi:10.1016/j.optcom.2019.02.020

https://hdl.handle.net/10356/143027

https://doi.org/10.1016/j.optcom.2019.02.020

Super-collimation and negative refraction in hyperbolic Van der Waals superlattices

Kandammathe Valiyaveedu Sreekanth[1, 2*] and Robert E. Simpson[3*]

[1]*Division of Physics and Applied Physics, School of Physical and Mathematical Sciences, Nanyang Technological University, 21 Nanyang Link, Singapore-637371*

[2]*Centre for Disruptive Photonic Technologies, The Photonic Institute, 50 Nanyang Avenue, Singapore-639798*

[3]*Singapore University of Technology and Design, 8 Somapah Road, 487372, Singapore*

Abstract: In this paper, we investigate supercollimation and negative group refraction properties of Van der Waals crystals. Van der Waals crystals, such as Bi_2Se_3, show both type I and type II hyperbolic dispersion at terahertz (THz) frequencies. An all angle negative group index of refraction is observed at frequencies that exhibit type I hyperbolic dispersion. However, a negative group index of refraction is observed at higher angles in the type II spectral region. The supercollimation effect is achieved at the inversion point of type II and the Reststrahlen band, where the resonance cone angle is close to zero. We further show broadband tunable hyperbolic dispersion from THz to mid infrared frequencies and a widening of the negative group index spectral band using topological insulator- dielectric insulator based superlattice structures.

Keywords: Hyperbolic metamaterials, THz frequencies, Topological insulators, Negative refraction, Van der Waals crystals

*Corresponding authors: sreekanthkv@ntu.edu.sg, robert_simpson@sutd.edu.sg

1. Introduction

Hyperbolic metamaterials (HMMs) have attracted substantial attention over the past few years due to their extreme anisotropic permittivity and ease of fabrication using conventional thin film physical vapor deposition techniques [1]. HMMs are artificial uniaxial media that exhibit hyperbolic dispersion, which results from the different signs of dielectric constants in and out of the plane of the HMM layers. Importantly, HMMs support propagation of bulk plasmon polariton modes (high-k modes) across the structure with infinitely large momentum in the effective medium limit [2]. The exceptional properties of high-k modes associated with HMMs have been proposed for various applications such as subwavelength imaging [3-5], spontaneous emission enhancement [6-7], single photon sources [8], biosensing [9-10], perfect absorption [11-12], thermal emitters [13], and negative refraction [14-15].

It has been shown that different material combinations were required to realize hyperbolic metamaterials from ultraviolet (UV) to terahertz (THz) frequencies. In the UV and visible frequencies, the hyperbolic dispersion is usually achieved by combining noble metals, such as Au and Ag, and dielectrics such as SiO_2, Al_2O_3, MgF_2, TiO_2, Si and PMMA [16-20]. Since noble metal-based HMMs are severely limited due to the strong dispersive nature of metals at visible frequencies, TiN has been proposed to replace the metallic layers in visible photonics applications [21]. For infrared hyperbolic dispersion, noble metals are unsuitable due to their high reflectivity. Therefore, heavily doped oxide semiconductors, such as Al: ZnO, InGaAs, and SiC have been used as an alternative plasmonic material [14, -22]. Since graphene is a low-loss and tunable plasmonic material at both infrared and THz frequencies, graphene-dielectric stacks have been used to realize hyperbolic dispersion and active HMMs in those frequency bands [23-24]. In addition, reconfigurable HMMs have been demonstrated using tunable materials, such as electride materials [25], hexagonal boron nitride [26], and phase change oxides and chalcogenides [27-28].

Recently, topological insulators [29] have been investigated for active HMM applications. In particular, bismuth-based topological insulators (Tis) were theoretically proposed to realize hyperbolic dispersion at THz frequencies [30]. The layered TIs, such as Bi_2Se_3 and Bi_2Te_3, are characterized by unusual gapless edge or surface states and a full insulating gap in the bulk [31]. These TIs support hyperbolic phonon polaritons, which are highly directional and deeply subdiffractional modes. In addition, the dispersion relation of TI-based HMMs can be tuned by doping the surface states [30]. Such TI-based active HMMs may offer different venues for achieving high-speed dynamically tunable THz photonic devices.

Interestingly, in addition to a single resonance causing ε to be less than zero, optical anisotropy plays a major role in HMMs with negative refraction [14]. However, double resonances, ε and μ are simultaneously less than zero, and extreme nanofabrication techniques are required in thin wire- and split ring-based metamaterials to achieve negative refraction. Negative refraction at mid-infrared frequencies has been experimentally demonstrated using heavily doped oxide semiconductors-based HMMs [14]. In addition, tunable graphene-based HMMs have been investigated for negative refraction at THz frequencies [15].

In this paper, we numerically investigate supercollimation and negative refraction in Bi_2Se_3 at THz frequencies. Moreover, we show that the hyperbolic dispersion band can be tuned from THz to mid-infrared (M-IR) frequencies, whilst negative group index spectral band can be widened using Bi_2Te_3-GeTe based superlattice HMMs.

2. Results and discussion

Bi_2Se_3 is composed of Se-Bi-Se-Bi-Se quintuple atomic planes that are separated by insulating Van der Waals bonds. The layered structure is depicted in the inset of Fig. 1b. This layered structure exhibit strong anisotropy of their phonon modes. The dominant (x-y)-axis and z-axis phonon frequencies of Bi_2Se_3 are 1.92 THz and 4.05 THz, respectively [32]. Since

these phonon mode frequencies are separated by a factor of two, Bi_2Se_3 exhibits extremely anisotropic dielectric permittivity. The real part of the uniaxial permittivity components, $\varepsilon^x(\omega)$ and $\varepsilon^z(\omega)$ are indefinite for a certain range THz frequency band. That is, $\varepsilon^x(\omega)\cdot\varepsilon^z(\omega)<0$. As a result, Bi_2Se_3 exhibits hyperbolic dispersion at THz frequencies for transverse magnetic (TM) polarization, $\frac{(k^x)^2+(k^y)^2}{\varepsilon^z(\omega)}+\frac{(k^z)^2}{\varepsilon^x(\omega)}=\frac{\omega^2}{c^2}$ and supports hyperbolic phonon polaritons, which are deeply subdiffractional and highly directional collective modes [30].

To determine the uniaxial permittivity components of Bi_2Se_3, we use the following model [30],

$$\varepsilon^{\alpha}(\omega)=\varepsilon_{\infty}^{\alpha}+\sum_{j=1,2}\frac{\omega_{p,j}^{\alpha 2}}{\omega_{to,j}^{\alpha 2}-\omega^2-i\gamma_j^{\alpha}\omega}\quad,\ \alpha=x,z \qquad (1)$$

The parameters used in the calculations are, ε_{∞}^{x} = 29, ε_{∞}^{z} = 17.4, $\omega_{to,1}^{x}$ = 1.92 THz, $\omega_{p,1}^{x}$ = 21.1 THz, $\omega_{to,2}^{x}$ = 3.75 THz, $\omega_{p,2}^{x}$ = 1.65 THz, $\omega_{to,1}^{z}$ = 4.05 THz, $\omega_{p,1}^{z}$ = 8.5 THz, $\omega_{to,2}^{z}$ = 4.61 THz, $\omega_{p,2}^{z}$ = 4.67 THz and γ_j^{α} = 0.105 THz. The real and imaginary parts of permittivity components ($\varepsilon^x(\omega)$ and $\varepsilon^z(\omega)$) are shown in Fig. 1a and Fig. 1b, respectively. It is clear that the real permittivity components alter sign from positive to negative with frequency, whilst both imaginary components are always positive. In Fig. 1a (inset), regions A represents dielectric band ($\varepsilon^x(\omega)>0$ and $\varepsilon^z(\omega)>0$), region B represents type II hyperbolic band ($\varepsilon^x(\omega)<0$ and $\varepsilon^z(\omega)>0$), region C represents Reststrahlen band ($\varepsilon^x(\omega)<0$ and $\varepsilon^z(\omega)<0$) and region D represents type I hyperbolic band ($\varepsilon^x(\omega)>0$ and $\varepsilon^z(\omega)<0$). This implies that Bi_2Se_3 supports both type I and type II hyperbolic dispersion at THz frequencies, which is not possible using graphene-based HMMs [15]. In particular, type II hyperbolic dispersion has a maximum bandwidth of 2.14 THz,

which belongs to the bandwidth difference between two phonon frequencies at 1.91 THz and 4.05 THz. However, the Reststrahlen band (4.05 THz to 4.4 THz) and type I hyperbolic band (4.6 THz to 4.9 THz) are narrow with a bandwidth of 0.35 THz and 0.3 THz, respectively.

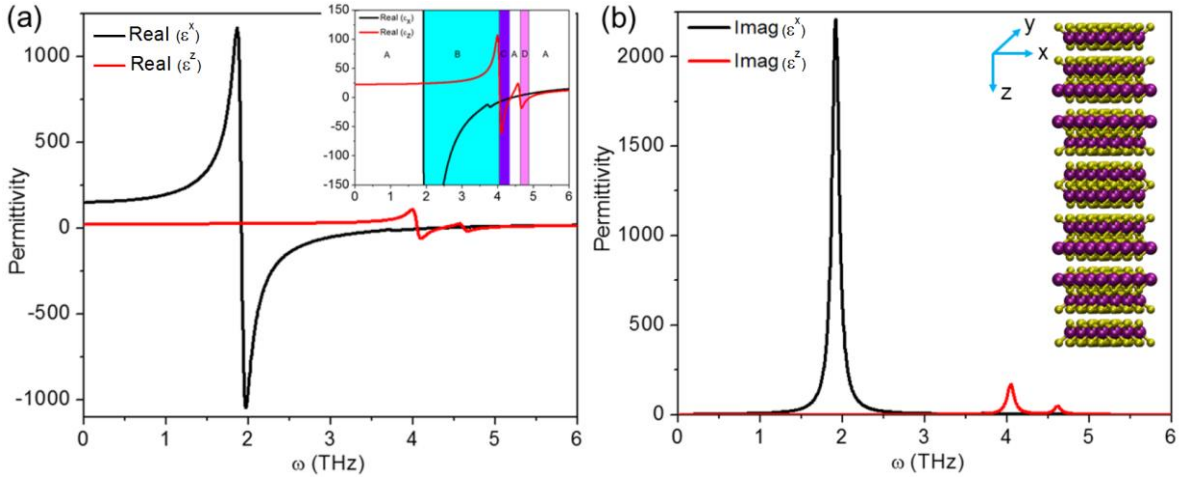

Figure 1. Frequency dependent uniaxial permittivity components ($\varepsilon^x(\omega)$ and $\varepsilon^z(\omega)$) of Bi_2Se_3 (a) real and (b) imaginary components. Inset of (b) represents the schematic of quintuple-layered Bi_2Se_3.

We now investigate negative refraction in Bi_2Se_3 in both the type I and type II hyperbolic bands. The Poynting vector (***S***), which points in the direction of energy flow and wavevector (***k***), directed along the wavefront normal are not parallel in anisotropic materials because the electric field vector (***E***) and electric displacement vector (***D***) are not parallel. These materials exhibit negative refraction with respect to ***S***, but positive refraction with respect to ***k*** when the boundary condition in which the tangential component of ***k*** is conserved at the interface [14]. Importantly, the directions of ***k*** and ***S*** depend on the effective phase (n_p) and group (n_g) indices of refraction, respectively. As a result, Bi_2Se_3 with indefinite permittivity ($\varepsilon^x(\omega)\cdot\varepsilon^z(\omega)<0$) exhibits negative refraction with respect to ***S*** for TM polarization. However, both ***k*** and ***S*** refract normally in the case of transverse electric (TE) polarization because the TE polarized light does not experience anisotropy. According to Snell's law, the effective phase and group indices of an anisotropic medium are related to

the angle of incidence (θ_{inc}). At low material absorption, phase and group indices can be obtained from [33],

$$n_p = \sqrt{\varepsilon^x + \left(1 - \frac{\varepsilon^x}{\varepsilon^z}\right)\varepsilon_0 \sin^2\theta_{inc}} \tag{2}$$

$$n_g = \frac{\varepsilon^z}{\varepsilon^x}\sqrt{\varepsilon^x - \frac{\varepsilon^x}{\varepsilon^z}\left(1 - \frac{\varepsilon^x}{\varepsilon^z}\right)\varepsilon_0 \sin^2\theta_{inc}} \tag{3}$$

where, ε_0 is the permittivity of the incident medium (air).

The calculated group and phase indices of refraction with angles of incidence are shown in Fig. 2a and Fig. 2b, respectively. It is evident that the group index is negative, and the phase index is positive in both type I and type II hyperbolic bands. It shows that Bi_2Se_3 exhibits negative refraction with respect to ***S*** and positive refraction with respect to ***k***, which allows forward wavefront propagation and negative energy refraction. In particular, all angle negative group index of refraction is obtained in the type I hyperbolic band, however, negative group index of refraction is obtained at higher incident angles (above 35°) in the type II hyperbolic band. This feature of negative refraction was previously predicted using a heavily doped oxide semiconductor-based type I HMM [14] and a type II graphene-based HMM [15]. It is important to note that Bi_2Se_3 shows both angle independence and angle dependent negative energy refraction due to the existence of both type I and type II hyperbolic bands respectively.

To further confirm the negative group index feature of Bi_2Se_3, the fraction of incident light reflected and transmitted at the air-Bi_2Se_3 interface as a function of incident angle was calculated by solving Fresnel's equations. A two-dimensional (2D) map of the reflection and transmission spectrum as a function of incident angle and frequency is shown in Fig. 2c and Fig. 2d, respectively. Note that both reflection and transmission TM polarized spectra were normalized with TE polarized spectra as TE polarized light does not experience the

anisotropy. The solid blue-yellow curve shown in Fig. 2c (ω <1.9 THz and ω >4.9 THz) shows the frequency dependence of the Brewster angle of TM-polarized light on the Bi2Se3 crystal, which is dielectric across this frequency band. Note, that an angular dependent discontinuity in the reflection (reflection peak) and transmission spectra (transmission dip) were obtained in the type I and type II hyperbolic bands. This was due to the negative group index of refraction of Bi_2Se_3 in both of these hyperbolic bands. Similar reflection and transmission spectral behavior were previously demonstrated using negative index HMMs [14-15]. Therefore, it can be concluded that the quintuple-layered Bi_2Se_3 provides extreme anisotropy and supports negative group index of refraction for TM polarization in hyperbolic bands.

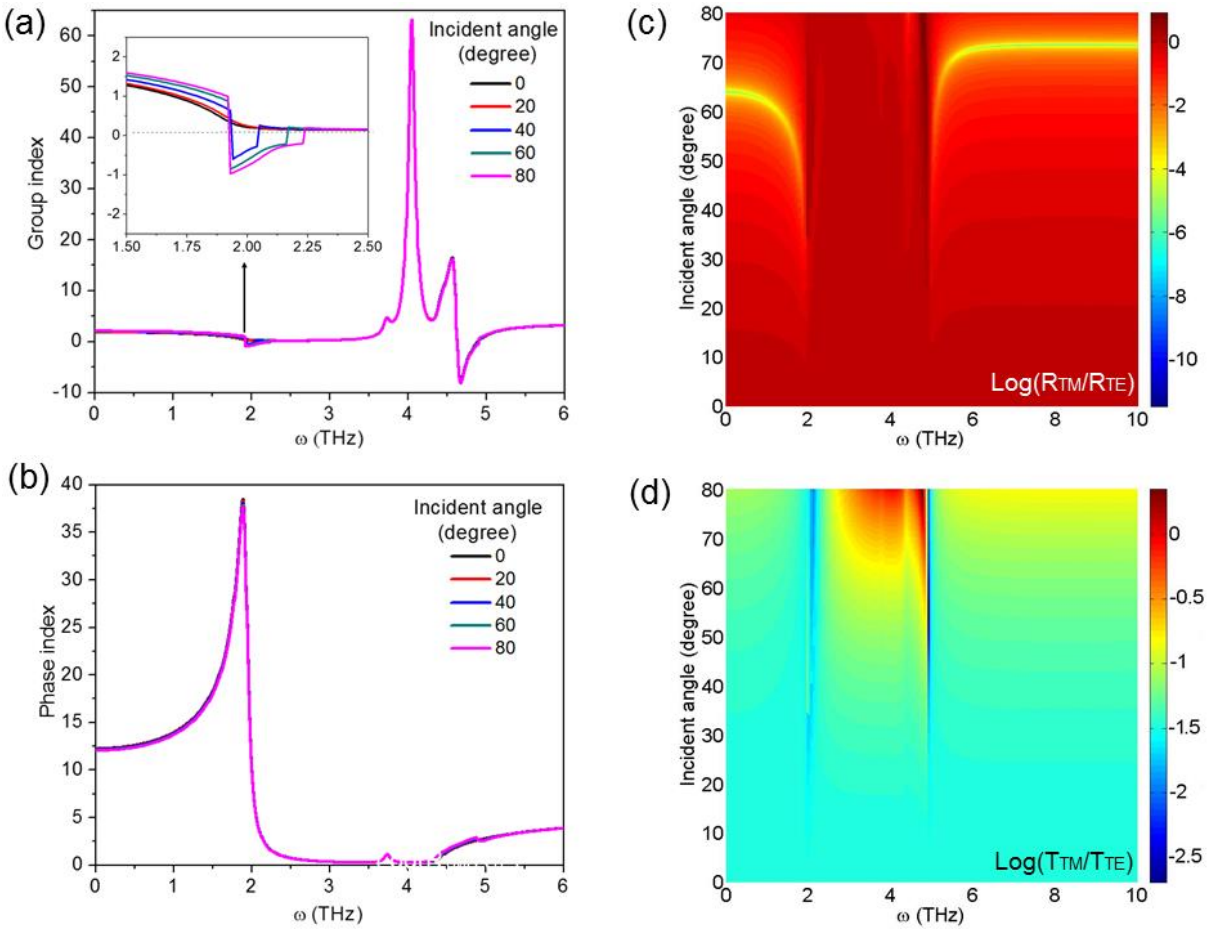

Figure 2. Frequency dependent (a) group and (b) phase indices of refraction with different angles of incidence. Two-dimensional map of (c) reflection and (d) transmission spectra as a function of incident angle and frequencies.

Since the hyperbolic phonon polariton mode supported by Bi_2Se_3 is highly directional and deeply subdiffractional, Bi_2Se_3 HMM can be used for super-collimation of light and super-lensing [3]. The propagation of wave inside HMM within the hyperbolic dispersion spectral band is allowed at the resonance cone (RC) angle. The half of the RC angle is given by, $\alpha_{RC} = a\tan\left[-(\varepsilon^x(\omega)/\varepsilon^z(\omega))^{1/2}\right]$. The condition for supercollimation of light is that when $\alpha_{RC} = 0$, which is possible either $\varepsilon^x(\omega) \approx 0$ or $\varepsilon^z(\omega) \approx \infty$. The calculated half of the RC angle for Bi_2Se_3 HMM is shown Fig. 3a. The minimum angle close to zero is obtained at the inversion point of type II and Reststrahlen band, which is at 4.05 THz.

The supercollimation effect and sub-wavelength focusing at terahertz frequencies is important for the realization of high resolution terahertz imaging devices for potential applications such as security screening, biodetection and weather navigation [34-35]. In order to verify the supercollimation properties of Bi_2Se_3 HMM at THz frequencies, we performed numerical simulation using 2D finite difference time domain (FDTD) method. In the simulation model, light coming from an 85 μm slit placed on top of the Bi_2Se_3 for different frequencies were analyzed. The quintuple-layered Bi_2Se_3 is considered as a single layer with thickness 150 nm and uniaxial permittivity components. The incident light was set to TM-polarization, and periodic and perfectly matched layer boundary condition was implemented along x and z-axis of the model, respectively. The propagation of plane wave at four different frequencies, corresponding to type II (3.5 THz), the inversion point of type II and Reststrahlen band (4.05 THz), the inversion point of Reststrahlen band and type I (4.6 THz) and type I (4.8 THz) were simulated and shown in Fig.3b. A line profile of normalized intensity recorded at bottom of the Bi_2Se_3 is shown in Fig. 3c. The supercollimation effect is evident at 4.05 THz where the RC angle is close to zero. It is also clear from the figures that intensity spectrum broadens with increase in RC angle.

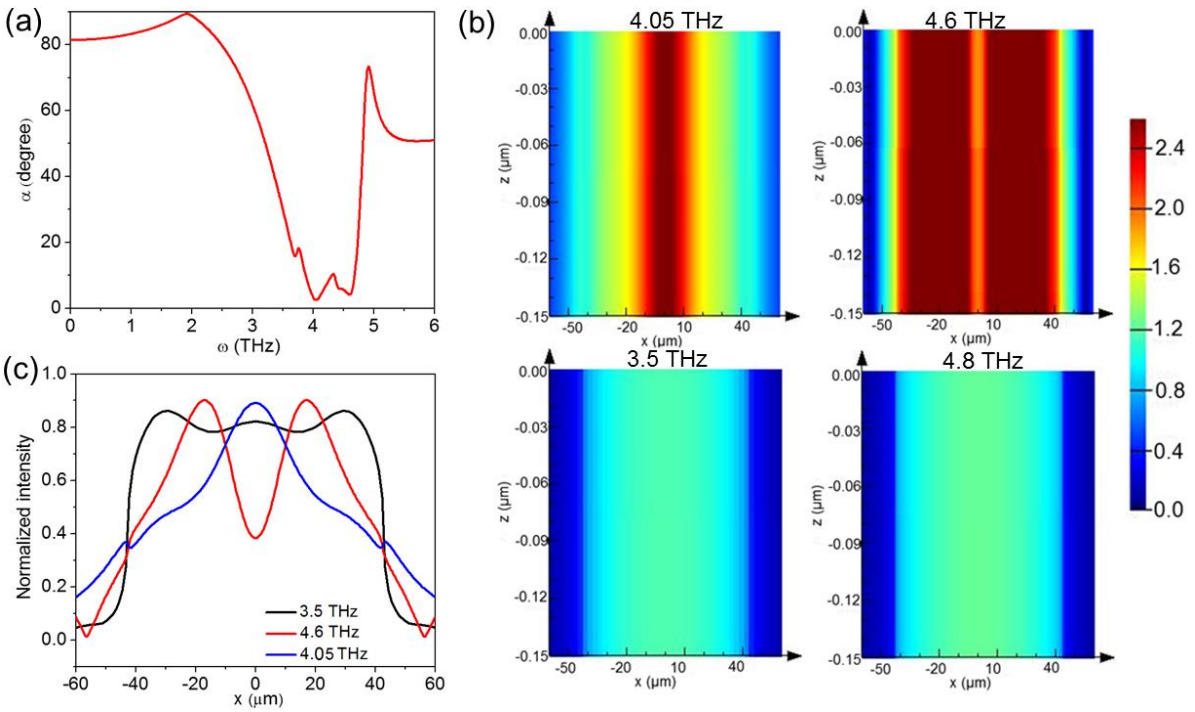

Figure 3. (a) Half of the resonance cone angle as a function of THz frequencies. (b) Propagation of plane wave through Bi_2Se_3 HMM at four THz frequencies. (c) Line profile of normalized intensity recorded at the bottom of quintuple-layered Bi_2Se_3.

The negative group index spectral band can be widened using topological insulator-dielectric insulator based superlattice structures. The proposed HMM superlattice structure comprises of alternating layers of Bi_2Te_3 and GeTe, which is shown in Fig. 4a (inset). The plasmons in topological insulator-dielectric insulator multilayer structures have been previously investigated [36]. The crystal structure of Bi_2Te_3 is similar to that of Bi_2Se_3 whilst GeTe is a phase change material. Indeed, these superlattice structures resemble the interfacial phase change material (iPCM) structure [37]. For the calculation of the HMM effective permittivity components, the permittivitties of Bi_2Te_3 were obtained from the Drude-Lorentz model, $\varepsilon(\omega) = \varepsilon_\infty - \frac{\omega_D^2}{\omega^2 + i\omega\gamma_D} + \sum_{j=1} \frac{\omega_{p,j}^2}{\omega_{0,j}^2 - \omega^2 - i\omega\gamma_j}$ with ε_∞ = 51, ω_D = 207.06 THz, γ_D = 5.507 THz, $\omega_{p,1}$ = 44.91 THz, $\omega_{0,1}$ = 2.0095 THz and γ_1 = 0.2998 THz. The dielectric permittivity of GeTe was considered as 15, which that of amorphous GeTe at THz frequencies [38] and the TI fill fraction was set to 0.35. As shown in Fig. 4a, the calculated real

uniaxial permittivitties of Bi_2Te_3-GeTe HMM demonstrates broadband type II hyperbolic dispersion from THz to M-IR frequencies, where $\varepsilon^x(\omega) < 0$ and $\varepsilon^z(\omega) > 0$.

In Fig. 4b, we show the calculated group index of refraction with different angles of incidence. It is clear from Fig. 4b that a negative group index of refraction is obtained at incident angles greater than 35° and the negative group index spectral band is widened with increasing angles of incidence. In contrast to Bi_2Se_3 HMM (Fig. 2a inset), a broad group index spectral band (2 to 5 THz) is obtained due to the broadband type II hyperbolic dispersion of the Bi_2Te_3-GeTe HMM. A 2D map of calculated fraction of incident light reflected at the air/Bi_2Te_3-GeTe HMM interface as a function of frequency and incident angle is shown in Fig. 4c. The obtained solid blue-yellow curve above 30 THz represents the Brewster angle condition for TM-polarization because Bi_2Te_3-GeTe HMM behaves as an isotropic dielectric medium above 30 THz. It is important to note that a discontinuity in the reflection spectra (reflection peak) with incident angle (35° to 80°) is obtained in the negative group index spectral band (2 to 5 THz). This spectral behavior matches very well with the discontinuity in the reflection spectra obtained in the type II hyperbolic band of the Bi_2Se_3 HMM (Fig. 2c).

An important advantage of the Bi_2Te_3-GeTe HMM is that the hyperbolic dispersion properties can be tuned by switching the structural phase of the GeTe from amorphous to crystalline. As shown in the inset of Fig. 4d, both type I and type II hyperbolic bands are present in Bi_2Te_3-GeTe HMM when the GeTe is in the crystalline phase. In the calculation, the dielectric permittivity of crystalline GeTe was 300 at THz frequencies [38]. The calculated group index is shown in Fig. 4d. It is important to note that the angle independent positive and negative group index is obtained in the type II and type I hyperbolic band, respectively. The positive group index obtained in the type II hyperbolic band is due to the fact that the uniaxial permittivity component, $\varepsilon^z(\omega)$ of crystalline Bi_2Te_3-GeTe HMM is

considerable larger after the GeTe amorphous to crystalline phase transition. This shows that the Bi_2Te_3-GeTe HMM is an alternative reconfigurable HMM for THz and mid infrared frequencies since the optical properties can be tuned by switching the phase of the GeTe from amorphous to crystalline as well as by doping the surface states of Bi_2Te_3.

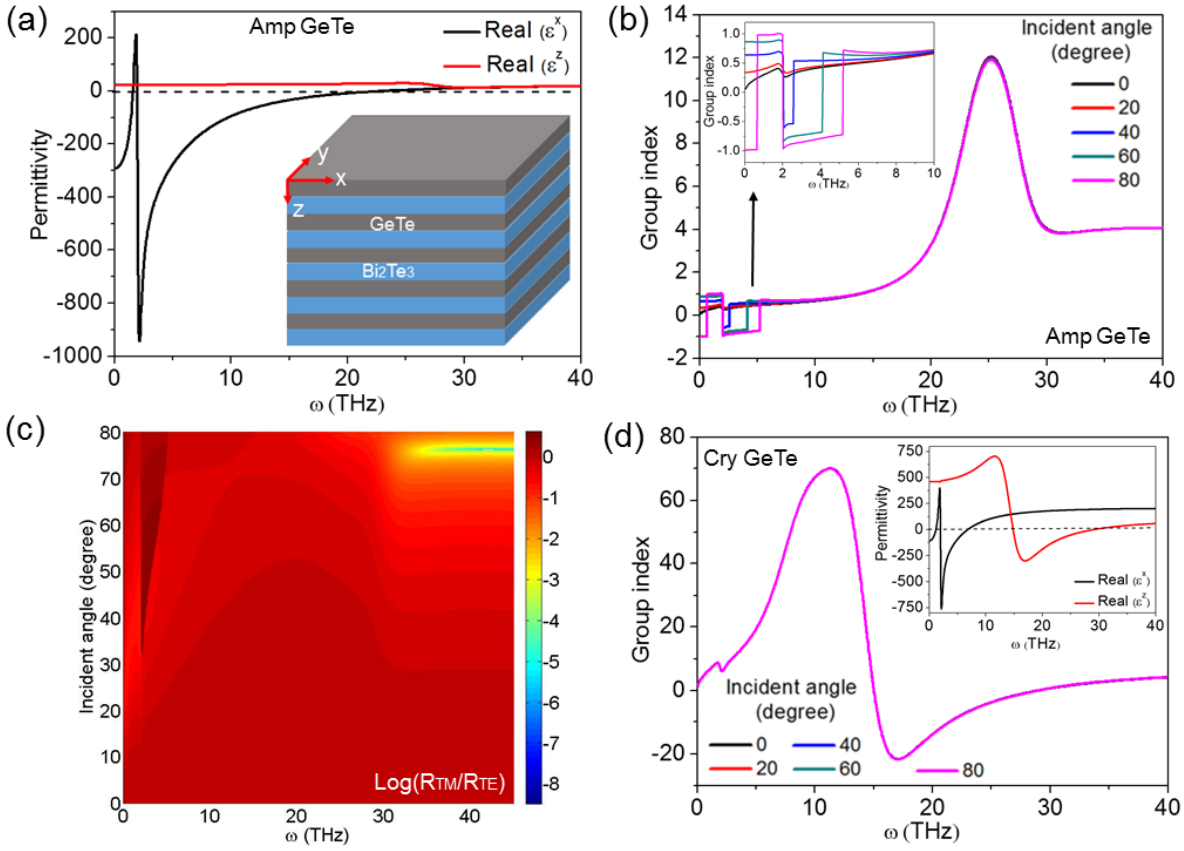

Figure 4. (a) Frequency dependent real uniaxial permittivity components of Bi_2Te_3-GeTe HMM. Inset shows the schematic of proposed Bi_2Te_3-GeTe HMM with GeTe is in amorphous phase. (b) Frequency dependent group index of refraction when GeTe is in amorphous phase. (c) Two-dimensional map of reflection spectra as a function of incident angle and frequencies. (d) Frequency dependent group index of refraction when GeTe is in crystalline phase.

3. Conclusion

In conclusion, the negative group index of refraction of the Bi_2Se_3 HMM was numerically analyzed. Since Bi_2Se_3 provides both type I and type II hyperbolic bands at THz frequencies, we showed that angle independent and angle dependent negative group index of refraction is possible in the type I and type II hyperbolic bands, respectively. The negative group index of

refraction properties was further confirmed by investigating the reflection and transmission spectra. Since highly directional hyperbolic phonon polaritons propagate within Bi_2Se_3 HMMs, we demonstrated that supercollimation of THz light is possible for a particular frequency where the resonance cone angle is close to zero. We further propose a tunable Bi_2Te_3-GeTe based superlattice HMM that exhibits a broadband hyperbolic dispersion from THz to M-IR frequencies. In the hyperbolic bands, this HMM showed an angle dependent broadband negative group index spectral band for the amorphous phase of GeTe and an angle independent positive and negative group index spectral band for the crystalline phase of GeTe. The presented results could be useful to design high resolution terahertz imaging devices as well as other applications.

Acknowledgements

This work was supported by the Singapore ministry of education Tier 2 project number T2MOE1713.

References

[1] L. Lu, R. E. Simpson, S. K. Valiyaveedu, Active hyperbolic metamaterials: progress, materials and design. J. Opt. 20 (2018) 103001.
[2] C. L Cortes, W. Newman, S. Molesky, Z. Jacob, Quantum nanophotonics using hyperbolic metamaterials. J. Opt. 14 (2012) 063001.
[3] V. Caligiuri, R. Dhama, K. V. Sreekanth, G. Strangi, A. De Luca, Dielectric singularity in hyperbolic metamaterials: the inversion point of coexisting anisotropies. Sci. Rep. 6 (2016) 20002.
[4] V. Caligiuri, A. De Luca, Metal-semiconductor-oxide extreme hyperbolic metamaterials for selectable canalization wavelength. J. Phys. D Appl. Phys. 49 (2016) 08LT01.
[5] V. Caligiuri, L. Pezzi, A. Veltri,A. De Luca. Resonant gain singularities in 1D and 3D metal-dielectric multilayered nanostructures. ACS Nano 11 (2017)1012-1025.
[6] H. Z. S. Krishnamoorthy, Z. Jacob, E. Narimanov, I. Kretzschmar, V. M. Menon, Topological transitions in metamaterials. Science 336 (2012) 205.
[7] K. V. Sreekanth, K. Hari Krishna, A. De Luca, G. Strangi, Large spontaneous emission rate enhancement in grating coupled hyperbolic metamaterials. Sci. Rep. 4 (2014) 6340.
[8] M. Y. Shalaginov, J. Liu, M. Ferrera, A. V. Akimov, A. Lagutchev, A. N. Smolyaninov, V. V. Klimov, J. Irudayaraj, A. V. Kildishev, A. Boltasseva, V. M. Shalaev, Enhancement of single-photon emission from nitrogen-vacancy centers with TiN/(Al,Sc)N hyperbolic metamaterial. Laser Photonics Rev. 9 (2015)120-127.
[9] K. V. Sreekanth, Y. Alapan, M. ElKabbash, E. Ilker, M. Hinczewski, U. A. Gurkan, A. De Luca, G. Strangi, Extreme sensitivity biosensing platform based on hyperbolic metamaterials. Nat. Mater. 8 (2016) 621-627.

[10] K. V. Sreekanth, Y. Alapan, M. ElKabbash, A. M. Wen, E. Ilker, M. Hinczewski, U. A. Gurkan, N. F. Steinmetz, G. Strangi, Enhancing the angular sensitivity of plasmonic sensors using hyperbolic metamaterials. Adv. Opt. Mater. 4 (2016) 1659.

[11] C. Guclu, S. Campione, F. Capolino, Hyperbolic metamaterial as super absorber for scattered fields generated at its surface. Phys. Rev. B 86 (2012) 205130.

[12] K. V. Sreekanth, M. ElKabbash, Y. Alapan, A. R. Rashed, U. A. Gurkan, G. Strangi, A multiband perfect absorber based on hyperbolic metamaterials. Sci. Rep. 6 (2016), 26272.

[13] Y. Guo, Z. Jacob, Thermal hyperbolic metamaterials. Opt. Exp. 21 (2013)15014-15019.

[14] A. J. Hoffman, L. Alekseyev, S. S. Howard, K. J. Franz, D. Wasserman, V. A. Podolskiy, E. E. Narimanov, D. L. Sivco, C. Gmachl, Nature Mater. 6 (2007) 946.

[15] K. V. Sreekanth, A. De Luca, G. Strangi, Negative refraction in graphene-based hyperbolic metamaterials. Appl. Phys. Lett. 103 (2013) 023107.

[16] Z. Jacob, I. I. Smolyaninov, E. E. Narimanov, Broadband Purcell effect: Radiative decay engineering with metamaterials. Appl. Phys. Lett. 100 (2012)181105.

[17] K. V. Sreekanth, T. Biaglow, G. Strangi, Directional spontaneous emission enhancement in hyperbolic metamaterials. J. Appl. Phys. 114 (2013)134306.

[18] K. V. Sreekanth, A. De Luca, G. Strangi, Experimental demonstration of surface and bulk plasmon polaritons in hypergratings. Sci. Rep 3 (2013) 3291.

[19] T. Xu, A. Agrawal, M. Abashin, K. J. Chau, H. J. Lezec, All-angle negative refraction and active flat lensing of ultraviolet light. Nature 497 (2013) 470.

[20] T. U. Tumkur, L. Gu, J. K. Kitur, E. E. Narimanov, M. A. Noginov, Control of absorption with hyperbolic metamaterials. Appl. Phys. Lett. 100 (2012)161103.

[21] G. V. Naik, B. Saha, J. Liu, S. M. Saber, E. A. Stach, J, M. K. Irudayaraj, T. D. Sands, V. M. Shalaev, A. Boltasseva, Epitaxial superlattices with titanium nitride as a plasmonic component for optical hyperbolic metamaterials. Proc. Natl. Acad. Sci. U S A 111 (2014) 7546-51.

[22] A. Boltasseva, H. A. Atwater, Low-loss plasmonic metamaterials. Science 331 (2011) 290-291.

[23] Y.C. Chang, C. H. Liu, C. H. Liu, S. Zhang, S. R. Marder, E. E. Narimanov, Z. Zhong, T. B. Norris, Realization of mid-infrared graphene hyperbolic metamaterials. Nat. Commun. 7 (2016)10568.

[24] I. V. Iorsh, I. S. Mukhin, I. V. Shadrivov, P. A. Belov, Y. S. Kivshar, Hyperbolic metamaterials based on multilayer graphene structures. Phys. Rev. B 87 (2013) 075416.

[25] S. Guan, S. Y. Huang, Y. Yao, S. A. Yang, Tunable hyperbolic dispersion and negative refraction in natural electride materials. Phys. Rev. B 95 (2017)165436.

[26] S. Dai, Q. Ma, M. K. Liu, Z. Fei, M. D. Goldflam, M. Wagner, K. Watanabe, T. Taniguchi, F. Thiemens, F. Keilmann, G. C. A. M. Janssen, S. E. Zhu, P. Jarillo-Herrero, M. M. Fogler, D. N. Basov, Graphene on hexagonal boron nitride as a tunable hyperbolic metamaterial. Nat. Nanotech. 10 (2015) 682-686.

[27] H. N. S. Krishnamoorthy, Y. Zhou, S. Ramanathan, E. Narimanov, V. M. Menon, Tunable hyperbolic metamaterials utilizing phase change heterostructures. Appl. Phys. Lett. 104 (2014)121101.

[28] S. Prayakarao, B. Mendoza, A. Devine, C. Kyaw, R. B. van Dover, V. Liberman, M. A. Noginov, Tunable VO2/Au hyperbolic metamaterial. Appl. Phys. Lett. 109 (2016) 061105.

[29] P. Di Pietro, M. Ortolani, O. Limaj, A. Di Gaspare, V. Giliberti, F. Giorgianni, M. Brahlek, N. Bansal, N. Koirala, S. Oh, P. Calvani, S. Lupi, Observation of Dirac plasmons in a topological insulator. Nat. Nanotech. 8 (2013) 556-560.

[30] J.-S. Wu, D. N. Basov, M. M. Fogler, Topological insulators are tunable waveguides for hyperbolic polaritons. Phys. Rev. B 92 (2015) 205430.

[31] M. Z. Hasan, C. L. Kane, Colloquium: Topological insulators. Rev. Mod. Phys. 82 (2010) 3045.
[32] W. Cheng, S.-F. Ren, Phonons of single quintuple Bi2Te3 and Bi2Se3 films and bulk materials. Phys. Rev. B 83 (2011) 094301.

[33] A. J. Hoffman, A. Sridhar, P. X. Braun, L. Alekseyev, S. S. Howard, K. J. Franz, L. Cheng, F. S. Choa, D. L. Sivco, V. A. Podolskiy, E. E. Narimanov, C. Gmachl, Midinfrared semiconductor optical metamaterials. J. Appl. Phys. 105 (2009)122411.

[34] A. Kannegulla, L. J. Cheng, Subwavelength focusing of terahertz waves in silicon hyperbolic metamaterials. Opt. Lett. 41 (2016) 3539-3542.

[35]C. M. Watts, D. Shrekenhamer, J. Montoya, G. Lipworth, J. Hunt, T. Sleasman, S. Krishna, D. R. Smith, W. J. Padilla, Terahertz compressive imaging with metamaterial spatial light modulators. Nat. Photon. 8 (2014) 605-609.
[36] Y. P. Lai, I. T. Lin, K. H. Wu, J. M. Liu, Plasmonics in topological insulators. Nanomater Nanotechnol 4 (2014) 13 doi: 10.5772/58558.
[37] R. E. Simpson, P. Fons, A. V. Kolobov, M. Krbal, T. Yagi, J. Tominaga, Interfacial phase-change memory. Nat. Nanotech. 6 (2011) 501-505.
[38] F. Kadlec, C. Kadlec, P. Kuzel, Contrast in terahertz conductivity of phase-change materials. Solid State Communications 152 (2012) 852-855.